NUCLEIC ACID THERAPEUTICS
Volume 25, Number 4, 2015

DOI: 10.1089/nat.2014.0525

RNA Nanoparticles Derived from Three-Way Junction of Phi29 Motor pRNA Are Resistant to I-125 and Cs-131 Radiation

Hui Li,[1,2] Piotr G. Rychahou,[3] Zheng Cui,[2] Fengmei Pi,[1,2] B. Mark Evers,[4] Dan Shu,[1,2,4] Peixuan Guo,[1,2,4] and Wei Luo[5]

Radiation reagents that specifically target tumors are in high demand for the treatment of cancer. The emerging field of RNA nanotechnology might provide new opportunities for targeted radiation therapy. This study investigates whether chemically modified RNA nanoparticles derived from the packaging RNA (pRNA) three-way junction (3WJ) of phi29 DNA-packaging motor are resistant to potent I-125 and Cs-131 radiation, which is a prerequisite for utilizing these RNA nanoparticles as carriers for targeted radiation therapy. pRNA 3WJ nanoparticles were constructed and characterized, and the stability of these nanoparticles under I-125 and Cs-131 irradiation with clinically relevant doses was examined. RNA nanoparticles derived from the pRNA 3WJ targeted tumors specifically and they were stable under irradiation of I-125 and Cs-131 with clinically relevant doses ranging from 1 to 90 Gy over a significantly long time up to 20 days, while control plasmid DNA was damaged at 20 Gy or higher.

Introduction

Cancer is a broad class of diseases featuring uncontrollable cell growth, invasion, and destruction of nearby tissues and metastasis [1,2]. Cancer has become one of the leading causes of death in the world, accounting for about 7.6 million deaths in 2008 [3]. The economic burden of cancer is also very high, to both the person with cancer and for the whole society. According to the estimation by the National Institutes of Health (NIH), the overall annual cost of cancer in 2008 was $201.5 billion [4]. Thus, an effective, efficient, and safe treatment for cancer is urgently needed.

Radiation therapy represents a major modality for anticancer therapy, which utilizes ionizing radiation produced by linear accelerators (external beam therapy) or radioactive isotopes (brachytherapy and nuclear medicine) to kill cancer cells, inhibit tumor growth, and prevent recurrence of the tumor [5]. However, radiation not only kills cancer cells but also damages healthy cells. The side effects associated with current radiation therapy significantly limit the doses delivered to the patients [6,7]. The goal of radiation therapy is to deliver a high dose of radiation to the target to kill cancer cells, while sparing the surrounding healthy tissues. However, this is not easy to achieve using current techniques. Medical imaging, including CT and MRI, is used to accurately identify and locate or track tumor before, during, and even after treatment. Since such imaging can only recognize balky lesions, it is very difficult to find and locate all the cancer cells, especially microscopic disease. In addition, it is also very difficult to avoid normal tissue damages during dose delivery. External beam therapy uses ionization particles that may have to pass through the normal tissue before reaching the target. Brachytherapy handles radiation sources mechanically and has significant uncertainty in localizing the radioactive sources. Although certain ionizing radiopharmaceuticals, such as I-131 and Y-90 used in nuclear medicine, can target certain organs and tumors, variation in biodistribution caused by metabolism and excretion of the pharmaceuticals and localization errors produces uncertainties and limitations in targeting tumor and dosimetry and, thus, increases damages to normal tissues [8].

Recently, nanoparticles have been found to be able to accurately target cancer cells and thus can be used for cancer targeting and treatment [9–14]. Nanoparticles are typically within several hundred nanometers in size and are comparable to large biological molecules such as enzymes, receptors, and antibodies. Due to the small size, nanoparticles can interact with biomolecules, both on the surface and inside the

[1]Nanobiotechnology Center, University of Kentucky, Lexington, Kentucky.
[2]Department of Pharmaceutical Sciences, College of Pharmacy, University of Kentucky, Lexington, Kentucky.
[3]Department of Surgery, Markey Cancer Center, University of Kentucky, Lexington, Kentucky.
[4]Markey Cancer Center, University of Kentucky, Lexington, Kentucky.
[5]Department of Radiation Medicine, Markey Cancer Center, University of Kentucky, Lexington, Kentucky.

cells, participate in molecular, biochemical, and biological processes, and thus can be used as agents for medical imaging and targeted cancer treatment [15]. The well-studied nanoparticles include quantum dots, carbon nanotubes, paramagnetic nanoparticles, liposomes, gold nanoparticles, and many others. However, there are concerns regarding the biocompatibility of these nanoparticles, especially when they are exposed to radiation and their ability to escape the reticuloendothelial system, which could lead to short- and long-term toxicity [16,17].

A new discovery in nanotechnology has led to the development of novel RNA nanoparticles mainly composed of RNA, which are capable of strongly binding to tumors without accumulation in other vital organs or tissues [18–20]. Since the first proof of concept in 1998 [21], RNA nanotechnology has emerged as a popular and rapidly growing field that is at the interface of nanotechnology, molecular biology, medicine, and biomedical engineering [13,20,22–26]. RNA nanotechnology holds significant translational potential in medicine and features that could make RNA nanoparticles as desired pharmaceutical agents and radioisotope carriers. First, RNA nanoparticles can be produced with a known stoichiometry and high reproducibility [21,26,27]. The simplicity of RNA, being composed of only four nucleic acid bases, allows for predictable and addressable formation of various nanostructures harboring different functional groups by bottom-up self-assembly. Second, RNA nanoparticles can target specific cell groups by targeting cell surface receptors through the use of RNA aptamers that function like protein or chemical ligands [18, 28, 29]. These structures do not induce antibody production, allowing for repeated delivery and therapy [28]. Third, RNA nanoparticles that have been produced have a size range of 10–50 nm, which is the perfect size not only to be retained within the body by avoiding rapid renal excretion but also to pass through leaky blood vessels in cancer tumors, as well as cell membranes, by cell surface receptor-mediated endocytosis [18–20].

To have clinical applications, RNA nanoparticles and those properties must remain stable and unchanged under the clinical conditions. The bacteriophage phi29 packaging RNA (pRNA) represents an attractive platform for bottom-up assembly of RNA nanoparticles [18–20]. The molecular structure of pRNA contains a helix domain, a central domain containing right- and left-hand loops, and a three-way junction (3WJ) core [30]. A recent study has indicated that the pRNA 3WJ has thermodynamic stability, and RNA nanoparticles constructed based on the pRNA 3WJ core are also thermodynamically and chemically stable [27]. In addition, the receptor-binding ligand, aptamer, short interfering RNA, or ribozyme can be incorporated into the pRNA 3WJ nanoparticle and can retain their correct folding and function. The pRNA nanoparticles also display a favorable pharmacokinetic profile for *in vivo* targeted delivery [half-life of 5–10 h compared to 0.25–0.75 h of 2′ fluorine (2′F) siRNA counterparts] [28]. To be used as radioisotope carriers, the stability of RNA nanoparticles should be further tested under irradiation with clinically relevant doses.

We have proposed to use the 3WJ RNA nanoparticles to carry radioisotope I-125 or Cs-131 so that cancer cells can be targeted by RNA nanoparticles and treated by I-125 or Cs-131. In nuclear medicine, several radioactive isotopes, such as I-131, P-32, and Y-90, have been used for targeted radionuclide therapy, but those isotopes are only applied to very limited types of cancer [31–35]. In addition, most of the isotopes used for nuclear medicine therapy are beta-emitters and not suitable for imaging. Accurate dose estimation is almost impossible without accurate imaging. On the other hand, I-125 and Cs-131 have been widely used in permanent implant brachytherapy and have successfully treated various types of cancer. The idea of using I-125 or Cs-131 with 3WJ RNA nanoparticles is to increase the accuracy of tumor targeting and enhance the effectiveness in treating a broad range of tumors and sparing normal tissues. In addition, both I-125 and Cs-131 emit photons that will help with *in vivo* nuclear imaging and studying the biodistribution of those isotopes for estimation of a patient-specific dose. As the first step, we investigated the stability of the pRNA 3WJ nanoparticles that are essential for *in vivo* cancer targeting and treatment in this study.

Materials and Methods

Oligonucleotides and assembly of RNA 3WJ nanoparticles

The RNA oligonucleotides used in this study for constructing the RNA 3WJ nanoparticles were ordered from TriLink BioTechnologies. Assembly of RNA 3WJ nanoparticles was performed by mixing equal molar concentrations of corresponding strands (3WJa: UUGCCAUGUGUAUGUGGG; 3WJb: CCCACAUACUUUGUUGAUCC; and 3WJc: GGAU CAAUCAUGGCAA) in a TMS (50 mM TRIS pH = 8.0, 100 mM NaCl, 10 mM $MgCl_2$) buffer. The 3WJ formations were confirmed on a 12% native polyacrylamide gel electrophoresis (PAGE) with a running buffer (89 mM Tris, 200 mM borate acid, and 5 mM $MgCl_2$) according to the published procedure [27]. Gels were stained with ethidium bromide (EB) or SYBR Green II and imaged by Typhoon FLA 7000 (GE Healthcare). The assembled RNA 3WJ nanoparticles were stored in a −20°C freezer before further characterization.

Atomic force microscopy imaging

Atomic force microscopy (AFM) was used to study the shape and size of 3WJ-pRNA nanoparticles harboring three monomeric pRNA [27]. AFM images were obtained by imaging the nanoparticles using specially modified mica surfaces (APS mica) [36] with a Veeco MultiMode AFM NanoScope IV system (Veeco/Digital Instruments), operating in the tapping mode, according to the method previously reported [27].

Temperature gradient gel electrophoresis

The thermodynamic stability of 2′F U/C-modified RNA 3WJ nanoparticles was studied using the temperature gradient gel electrophoresis (TGGE) system (Biometra GmbH). The 2′F U/C-modified RNA oligonucleotides used in this study for constructing the RNA 3WJ nanoparticles were ordered from TriLink BioTechnologies. The 3WJb strand was 5′-end γ-32P ATP-labeled (PerkinElmer) prior assembly. Assembly of RNA 3WJ nanoparticle was achieved by mixing 10 μM total RNA strands in the TMS buffer, heating to 80°C, and cooling it down to 4°C over 1 h. RNA nanoparticles were subjected to a 15% native PAGE (2.5 μL of RNA per well)

and allowed to run for 10 min at ambient temperature at constant 100 V. After RNA entered into the gel matrix, the gel was transferred into a TGGE apparatus and a linear temperature gradient was set up from 36°C to 80°C perpendicular to the electrical current. The gel was run at 100 V for 1 h and then was dried under vacuum and imaged using a phosphor storage screen with Typhoon FLA 7000 (GE Healthcare).

Confocal microscopy of HT29 colon cancer cells incubated with RNA nanoparticles

Colon cancer HT29 cells were plated on coverslips (Fisher Scientific) with a folate-free medium in a 24-well plate and cultured at 37°C in humidified air containing 5% CO_2 overnight. The cells were washed with the folate-free medium twice to remove dead cells. The Alexa-647-labeled folate-3WJ and folate-free 3WJ 2′F RNA nanoparticles were diluted to 200 nM in the folate-free medium and incubated with the cells at 37°C for 2 h. After washing with a phosphate-buffered saline (PBS), the cells were fixed with 4% paraformaldehyde, stained with Alexa Flour®488 Phalloidin (Life technologies Corporation) for actin, and ProLong® Gold Antifade Reagent with DAPI (Life technologies) for the nucleus. The images were taken on an Olympus FV1000 confocal microscope (Olympus Corporation).

Flow cytometry analysis of cellular binding of RNA nanoparticles

KB cells were cultured in the folate-free RPM1-1640 medium (Gibco), then digested with trypsin, and rinsed with the folate-free medium. Three nanomolars of the Alexa 647-labeled 3WJ-folate and 3WJ 2′F RNA were incubated with 2×10^5 KB cells at 37°C for 1 h. After washing with PBS twice, the cells were resuspended in 200 μL of the PBS buffer for flow cytometry analysis. Fluorescence intensity was determined with a FACSCalibur flow cytometer (BD Biosciences) by counting 20,000 events each sample.

Cytotoxicity assay

The cytotoxicity of RNA nanoparticles was evaluated with an MTT assay kit (Promega) following the manufacturer's instruction. Briefly, HT29 cells were plated in a 96-well plate and cultured at 37°C in humidified air containing 5% CO_2 overnight. The folate-3WJ 2′F RNA nanoparticles were suspended in fresh McCoy's 5A with a 10% fetal bovine serum (FBS) medium at the indicated concentrations and added to the cells for incubation at 37°C for 24 h. Then, 15 μL of dye solution was added to each well and incubated at 37°C for 4 h; 100 μL of solubilization/stop solution was added to each well and incubated at room temperature for 2 h for color development. The absorbance at 570 nm was recorded using a microplate reader (Synergy 4; BioTek Instruments, Inc.). The cell viability was calculated relative to the absorbance of cells in only control (viability of cells in only control = 100%).

Animal trial: in vivo *cancer targeting of RNA 3WJ nanoparticles*

To evaluate the cancer-targeting property of RNA 3WJ nanoparticles, an animal trial was conducted. All experiments involving animals are approved by the University of Kentucky Institutional Animal Care and Use Committee (IACUC). Male athymic nude nu/nu (6–8 week old) mice were obtained from Taconic and housed in clean pathogen-free rooms in an environment with controlled temperature (27°C), humidity, and a 12-h light/12-h dark cycle. The mice were fed standard chow and tap water ad libitum and allowed to acclimate for 1 week. HT29 colon cancer tumor cells were injected subcutaneously (10×10^6 cells in 100 μL 1× PBS). RNA nanoparticles were administered intravenously 1 week after tumor cell injection. The folate and Alexa 647-labeled 2′F U/C-modified RNA oligo strands for assembling the RNA 3WJ nanoparticles were custom ordered from TriLink BioTechnologies, Inc. Mice were fed a folate-free diet (Harlan Laboratories) for a total of 1 week before the folate-pRNA 3WJ nanoparticles were injected. For intravenous injection, mice were anesthetized using isoflurane gas (2% in oxygen at 0.6 L/min flow rate) and injected with 50 μg (2 mg/kg) of 2′F U/C-modified folate Alexa 647-labeled pRNA 3WJ nanoparticles in 300 μL of PBS; second injection of 50 μg (2 mg/kg) 2′F U/C-modified folate-Alexa 647-labeled pRNA 3WJ nanoparticles in 300 μL of PBS was administered 3 h later. CO_2 asphyxiation was performed by 6 h after first injection. Following CO_2 asphyxiation, the organs and tumors of the mice were dissected. Organ and tumor imaging (Alexa Fluor 647, Ex = 640 nm, Em = 680 nm) was carried out on the IVIS Spectrum station (Caliper Life Sciences) 6 h after the first injection. Composite images obtained comprised black and white digital photos with an overlay of images reflecting a fluorescent activity. The density map, measured as photons/second/cm^2/steradian, was created using the Living Image 3.1 (Caliper Life Sciences) software and represented as a color gradient centered at the maximal spot.

Urea stability assay

Urea is a denaturing agent that is widely used in biochemistry to denature RNAs or proteins. Urea stability assays were performed to assay the stability of RNA 3WJ nanoparticles in the presence of urea. Urea stability was tested by mixing assembled RNA 3WJ nanoparticles with different concentrations of urea (2, 4, 6, and 8 M). The samples were assayed on a 12% native PAGE, stained with EB, and imaged by Typhoon FLA 7000 (GE Healthcare).

FBS degradation assay

Stability of nanoparticles in the body is critical for its *in vivo* application, as many enzymes could degrade nanoparticles rapidly and hinder their application. In the blood, the instability of RNA is mainly the result of enzymatic degradation by ribonucleases (RNases). RNases can be divided into two major categories: endoribonucleases and exoribonucleases. Endoribonucleases cleave phosphodiester bonds within the RNA backbone, while exoribonucleases cleave phosphodiester bonds at either the 5′ end or the 3′ end of an RNA chain. RNA is indeed very sensitive to degradation by RNases, which confers a very short half-life, and thus, a poor pharmacokinetic profile for most RNA molecules. This limits the *in vivo* usage of RNA molecules as therapeutics. However, chemical modifications of RNA can overcome this shortcoming. For example, the substitution of the 2′ hydroxyl group with a 2′F atom dramatically increases the stability of RNA *in vivo* by preventing degradation by RNases [37–40].

To test the stability of RNA 3WJ nanoparticles with FBS treatment, assembled RNA 3WJ nanoparticles were incubated with 10% FBS in a 1640 cell culture medium in a 37°C water bath for different time up to 36 h. Samples were then assayed on a 12% native PAGE, stained with EB, and imaged by Typhoon FLA 7000 (GE Healthcare). ImageJ software was used to integrate the intensities of the assembled RNA 3WJ nanoparticles in the gel. Integration areas for each time point were compared to the integration area for the 0 min time point to construct a serum degradation comparison between the RNA and 2′F RNA nanoparticles. Origin 8.6 software was used to generate the plots.

Irradiation of RNA 3WJ nanoparticles with I-125 and Cs-131

Two brachytherapy sources were used in this study. I-125 is an isotope that is commonly used to treat prostate cancer and tumors in various sites. It decays into Te-125 with electron capture emitting photons with a broad spectrum whose mean energy is 28 keV; the half-life is 59.4 days. I-125 brachytherapy sources used in this study for prostate implants were produced by IsoAid as a cylindrical shape with a physical length of 4.5 mm and outer diameter of 0.8 mm; the I-125 material was coated onto a silver rod encapsulated with a thin titanium shielding [41].

Isotope Cs-131 is relatively new to brachytherapy, but has already been used for the treatment of various types of cancer such as prostate, breast, eye, and recent gynecological malignancies [42–47]. It is similar to I-125 in many aspects. It also decays in electron capture and emits photons with a mean energy of 30 keV, but the half-life of Cs-131 is only 9.7 days [48]. The Cs-131 source was provided by IsoRay Medical, Inc. as a small cylinder 4.5 mm in length and 0.8 mm in diameter.

I-125 or Cs-131 radioactive sources were immersed in the sample liquid (1 cc) contained in a small vial. The irradiation of the 2′F U/C-modified RNA samples was performed for different time periods and doses. The purpose was to distinguish the effects of radiation on DNA and RNA structures. Unirradiated samples were maintained in the same buffer and temperature and used as control. After irradiation, the integrity of the RNA 3WJ nanoparticles and plasmid control was assayed by 12% native PAGE with a TBM running buffer or 0.7% agarose gel with a TAE running buffer, respectively.

Results

RNA 3WJ nanoparticles form by one-pot self-assembly

RNA 3WJ consists of three fragments: $3WJ_a$, $3WJ_b$, and $3WJ_c$. RNA nanoparticles were formed by mixing three pieces of chemically synthesized oligos, $3WJ_a$, $3WJ_b$, and $3WJ_c$, at a 1:1:1 molar ratio (Fig. 1). The three pieces were assembled into nanoparticles very efficiently by simple mixing (Fig. 1C, lane 7), indicating the thermodynamically stable properties of the pRNA 3WJ. Notably, with the 1:1:1 ratio of 3WJa, 3WJb, and 3WJc, almost more than 90% or close to 100% of the three RNA fragments assembled efficiently into the 3WJ complex. This feature of efficient self-assembly [27] suggests that pRNA 3WJ nanoparticles can be fabricated very simply and easily, which is advantageous for therapeutic development and clinical translation. AFM imaging also confirmed the formation of 3WJ-pRNA nanoparticles harboring three monomeric pRNA and revealed the triangular branched structure of the nanoparticle with the size of 10–15 nm (Fig. 1B).

Folate-conjugated RNA nanoparticles bind to cancer cells specifically in vitro

The 2′F-modified 3WJ RNA nanoparticles conjugated with the folate were tested for specific binding and entry to colon cancer HT29 cells by confocal microscopy. In the folate-conjugated 3WJ RNA nanoparticles, the 3WJb strand was labeled with folate and the 3WJc strand was labeled with Alexa 647. 3WJ RNA nanoparticles without folate were used as a negative control. Confocal imaging indicated strong binding and entry of the folate-conjugated 3WJ nanoparticles to colon cancer HT29 cells, as demonstrated by colocalization of the nucleus stained by DAPI, actin stained by A488-phallodin, and Alexa 647-labeled RNA nanoparticle signals (Fig. 2A). Flow cytometry analysis indicated that folate-labeled 3WJ 2′F RNA nanoparticles can also bind to folate receptor overexpressed KB cells (Fig. 2B).

RNA 3WJ nanoparticles hold low cytotoxicity revealed in cell assay

The cytotoxicity of folate-3WJ 2′F RNA nanoparticles on colon cancer HT29 cells was evaluated with a standard colorimetric MTT assay that assesses the cell proliferation. We found that folate 3WJ 2′F RNA nanoparticles did not induce measurable cell viability loss on colon cancer HT29 cells even at a high concentration of 0.4 μM (Fig. 2C), indicating that the RNA nanoparticles are biocompatible and not toxic.

RNA 3WJ nanoparticles targeting xenograft cancer by systemic injection

Systemic injection of RNA 3WJ nanoparticles was used to confirm the chemical and thermodynamical stability and cancer targeting of these nanoparticles. Moreover, as a preliminary study to evaluate the feasibility of RNA nanoparticles to carry radioisotopes for cancer targeting *in vivo*, we used fluorescent dye instead of a radioisotope in a pilot experiment. RNA nanoparticles were constructed with one RNA fragment carrying folate as a cancer-targeting ligand and another RNA fragment carrying the Alexa 647 fluorescent probe instead of a radioisotope. The folate-3WJ RNA nanoparticles were systemically injected into mice through the tail vein, and 3WJ RNA nanoparticles without folate were used as control. Organ and tumor imaging by the IVIS Spectrum station 6 h after the first injection shows that the fluorescent signal was accumulated in the tumor specifically, but not in normal organs, including the liver and lung in the mice body (Fig. 2D), indicating that the folate-3WJ RNA nanoparticles targeted to the tumor and did not accumulate or become trapped in the liver and lung after systemic delivery.

Chemically modified RNA 3WJ nanoparticles are chemically and thermodynamically stable

In addition, we measured the thermodynamic stability of RNA 3WJ nanoparticles by TGGE (Fig. 1D). This technique allows the determination of melting temperatures of nucleic

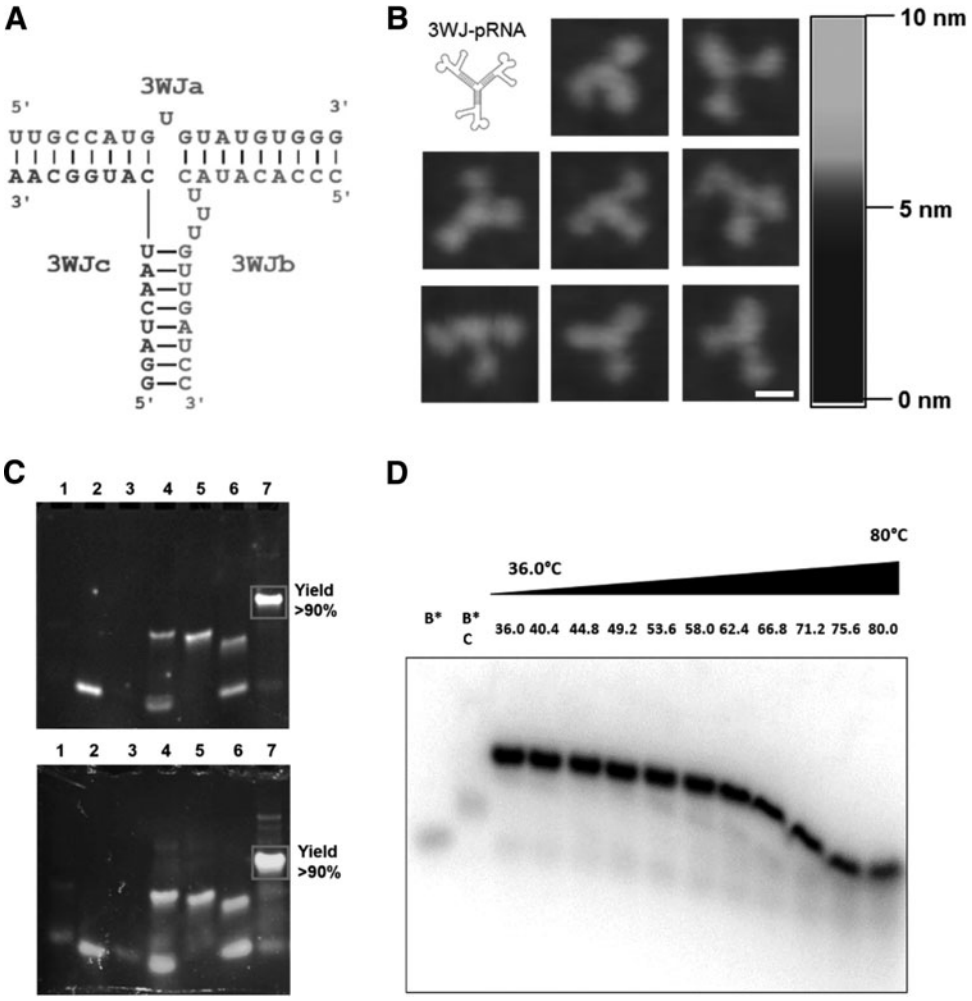

FIG. 1. Structure, assembly, and characterization of RNA 3WJ nanoparticles. **(A)** Secondary structure of the pRNA 3WJ. **(B)** Eight representative images of RNA 3WJ-pRNA nanoparticles are shown in magnified view and the images reveal a three-branch shape of the RNA nanoparticles. The AFM images of the RNA nanoparticles were obtained on APS-modified mica surface by a Veeco MultiMode AFM NanoScope IV system. (Scale bar: 10 nm). **(C)** Native PAGE (12%) demonstrates the stepwise assembly of RNA 3WJ nanoparticles, stained by ethidium bromide (*upper*) and SYBR Green II (*lower*). *Lane:* 1, $3WJ_a$; 2, $3WJ_b$; 3, $3WJ_c$; 4, $3WJ_a+3WJ_b$; 5, $3WJ_a+3WJ_c$; 6, $3WJ_b+3WJ_c$; 7, $3WJ_a+3WJ_b+3WJ_c$. **(D)** The thermodynamic stability of assembled RNA 3WJ nanoparticles was revealed by using the TGGE system. The temperature gradient was set from 36°C to 80°C, and the direction was set perpendicular to the electric field. The *left two lanes* are the 3WJ fragments, and the 3WJ complex starts at the third lane. 3WJ, three-way junction; AFM, atomic force microscopy; PAGE, polyacrylamide gel electrophoresis; pRNA, packaging RNA; TGGE, temperature gradient gel electrophoresis.

acids by means of decreasing the fraction of a nanoparticle with increasing temperature on PAGE [49,50] (Fig. 1D). The 2′F-modified 3WJ nanoparticles remained stable at a temperature as high as 66.8°C ± 2°C, which is above the temperature of the normal human body.

RNA 3WJ nanoparticles were mixed with 2, 4, 6, and 8 M urea and loaded into the TBM gel (Fig. 3A). In the presence of 8 M urea, assembled RNA 3WJ nanoparticles still showed little dissociation, which is in agreement with previously published results [27].

We also tested the stability of RNA 3WJ nanoparticles with up to 36 h of serum treatment (Fig. 3B). Previously published reports by Pieken *et al.* [37], Kawasaki *et al.* [38], Sabahi *et al.* [39], and Liu *et al.* [40] have demonstrated that 2′F-modified RNA has increased resistance to ribonuclease as well as enhanced thermodynamic stability. Our results showed the similar results for the RNA 3WJ nanoparticles. Specifically, unmodified RNA 3WJ nanoparticles were degraded in serum, which was revealed by the disappearance of the nonmodified RNA 3WJ nanoparticles after serum treatment, indicating that the majority of the unmodified RNAs were degraded. However, 2′F-modified RNA 3WJ nanoparticles were resistant to serum-induced degradation. In contrast to unmodified RNA nanoparticles, more than 90% of 2′F-modified RNA 3WJ nanoparticles remained intact after 36 h of serum treatment, which is in agreement with the published reports [27].

RNA 3WJ nanoparticles are stable under irradiation with I-125 and Cs-131

The stability of 2′F-modified RNA 3WJ nanoparticles under irradiation with clinically relevant doses was crucial

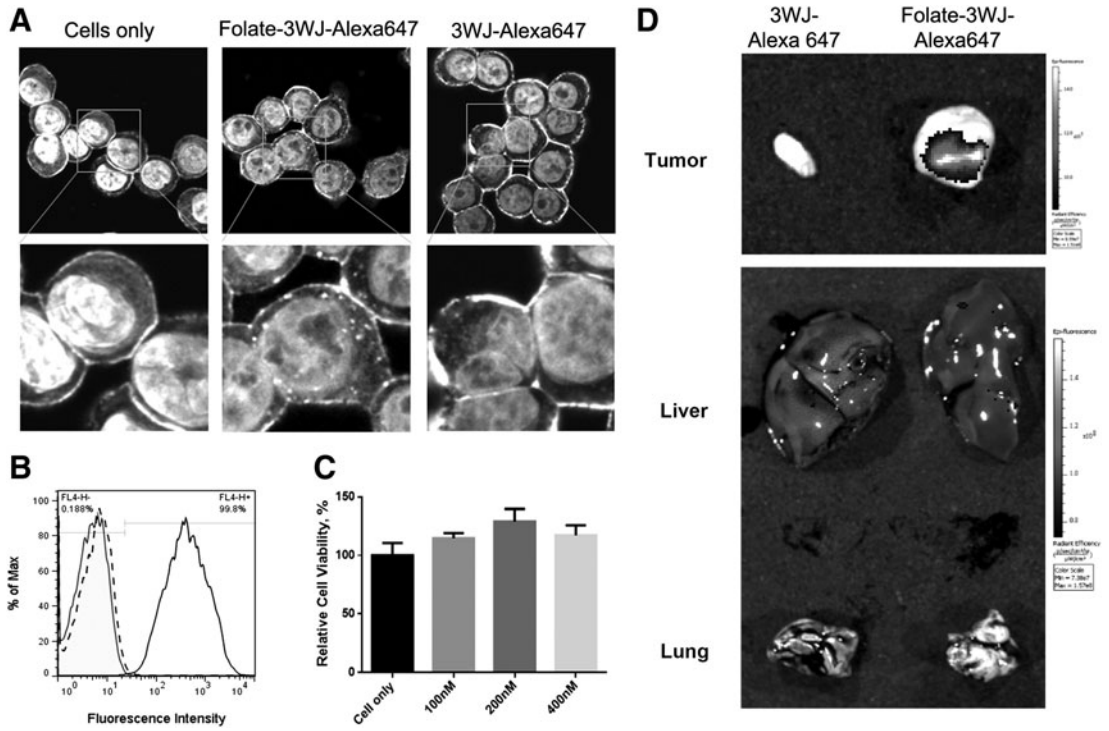

FIG. 2. Targeting, uptake, and cytotoxicity of RNA 3WJ nanoparticles. **(A)** Confocal images showing the uptake comparison of the folate-3WJ RNA nanoparticles and 3WJ-only RNA nanoparticles to colon cancer HT29 cells, enlarged micrograph showing punctate pattern of Alexa647 labeled RNA nanoparticles in HT29 cells. **(B)** Flow cytometry analysis showing the binding of folate-labeled 3WJ 2′F RNA nanoparticles to folate receptor overexpressed KB cells. *Tinted curve:* cell-only control; *dotted curve:* 3WJ RNA nanoparticles without folate; *black solid curve:* 3WJ RNA nanoparticles with folate. **(C)** Effect of the folate-3WJ RNA nanoparticles on HT29 cell viability. The cells were incubate with three different concentrations (100, 200, and 400 nM) of the folate-3WJ RNA nanoparticles. **(D)** The folate-3WJ-Alexa 647 nanoparticles were injected intravenously into nude mice with HT29 subcutaneous xenografts. Accumulation of fluorescently labeled folate-3WJ nanoparticles in the tumor, liver, and lung was evaluated by IVIS Spectrum station. 2′F, 2′ fluorine.

for the development of targeted radiation therapy. The stability tests were performed with I-125 and Cs-131 irradiation. DNA plasmids were included as control. The plasmid DNA we used was in the circular form. Cleavage of the circular plasmid at a random site will result in a linear DNA that migrates to different locations in the gel. Multiple cleavage of the DNA will result in random sizes that form a smear in the gel, and many individual bands with low concentrations were not visible since each DNA will have several thousand random cleavage sites. The test with I-125 was first performed for a low dose of 1 Gy to both RNA and DNA samples, but no change was observed. When the dose was increased to 30 Gy, a typical therapeutic dose, RNA 3WJ nanoparticles still remained unchanged (Fig. 3C), while DNA smear was formed as shown in Fig. 3D, which provided evidence of the cleavage of the plasmid DNA by radiation. The upper bands and lower bands in lane 1 and 3 represent linear and supercoiled plasmid DNA, respectively. These results are summarized in Table 1. Four tests were also conducted with Cs-131 for 7, 20, 30, and 90 Gy, and the irradiation lasted up to 20 days (longer than 2 half-life of 9.7 days). Both DNA and RNA structures were intact for 7 Gy, but DNA was broken while RNA 3WJ nanoparticles remained intact for 20 Gy or higher. The results are summarized in Table 2, and the result for 30 Gy is shown in Fig. 3D.

The results showed that RNA 3WJ nanoparticles were stable under irradiation of I-125 and Cs-131 with doses ranging from 1 to 90 Gy. However, the DNA plasmids were damaged with a dose of 20 Gy or higher, the therapeutic doses prescribed for cancer treatment, while the RNA 3WJ nanoparticles remained intact. This result has indicated that RNA 3WJ nanoparticles may be able to carry therapeutic doses of I-125 and Cs-131 for cancer treatment.

Discussion

RNA nanotechnology is an emerging field with increasing popularity among the scientific community [13,21,51–59]. RNA 3WJ-based nanoparticles have been successfully fabricated (Fig. 1) and share the advantages of a targeted drug delivery system of specific delivery and longer retention time, which reduce the dosage required and the side effects. The specific delivery can be achieved through the EPR (enhanced permeability and retention) effect or active targeting through conjugation with ligands such as the aptamer, folate, and RGD. Systemic injection of thermodynamically and chemically stable RNA nanoparticles into mice revealed that RNA nanoparticles strongly and specifically bound to cancers without accumulating in normal organs, including the liver and lung (Fig. 2D).

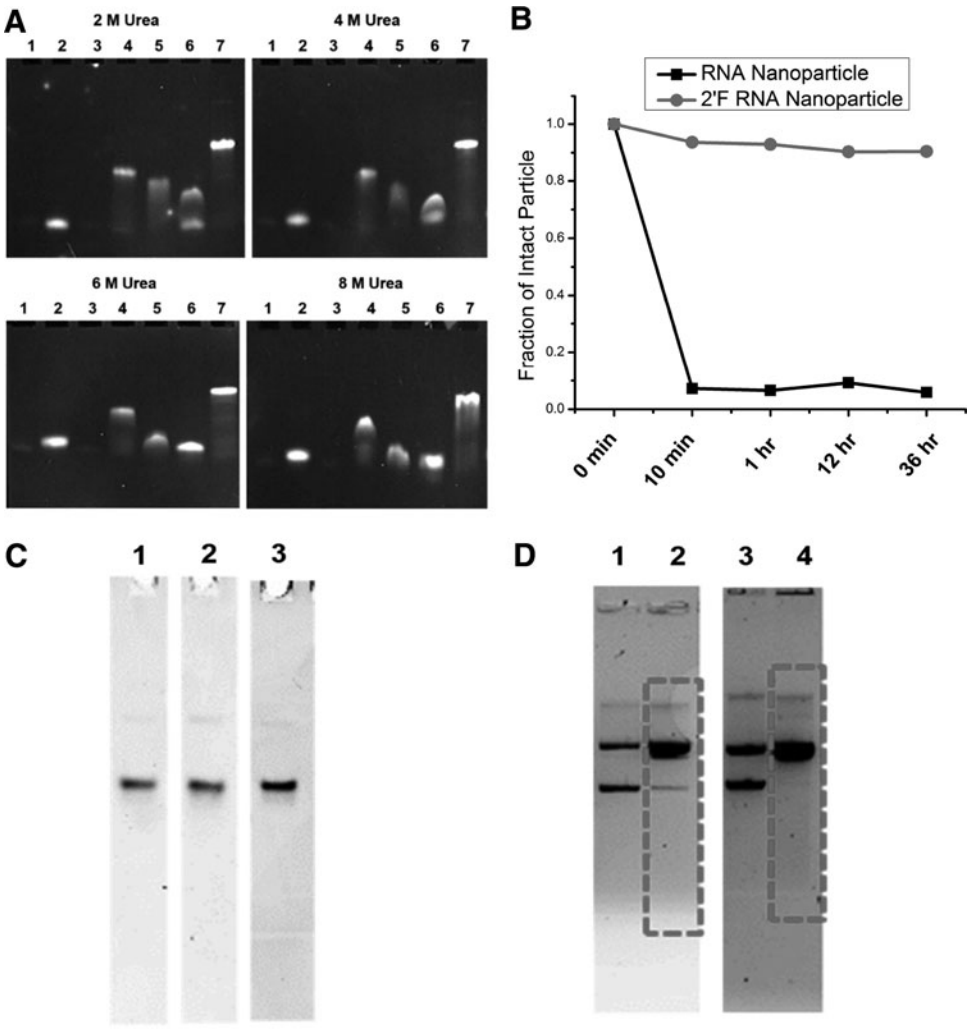

FIG. 3. Stability assay of RNA 3WJ nanoparticles for urea, serum, and irradiation. **(A)** Native PAGE (12%) demonstrates the stability of RNA 3WJ nanoparticles against 2–8 M urea denaturation. The gel was stained by ethidium bromide. *Lane:* 1, $3WJ_a$; 2, $3WJ_b$; 3, $3WJ_c$; 4, $3WJ_a+3WJ_b$; 5, $3WJ_a+3WJ_c$; 6, $3WJ_b+3WJ_c$; 7, $3WJ_a+3WJ_b+3WJ_c$. **(B)** Nanoparticle stability in serum was compared between 2′F-modified and nonmodified RNA 3WJ nanoparticles for up to 36 h. *Square:* RNA nanoparticle; *red sphere:* 2′F RNA nanoparticle. **(C)** RNA 3WJ nanoparticles were resistant to radiation. 2′F-modified RNA 3WJ nanoparticles were examined by 12% native PAGE with the TBM running buffer after 7-day irradiation with Cs-131 or 18-day irradiation with I-125. A dose of 30 Gy was given by both Cs-131 and I-125. No obvious change was detected after 7- or 18-day irradiation. *Lane:* 1, RNA nanoparticles without irradiation; 2, RNA nanoparticles after 7-day irradiation (30 Gy) with Cs-131; 3, RNA nanoparticles after 18-day irradiation (30 Gy) with I-125. **(D)** Plasmid DNA was damaged by radiation. Plasmid DNA was examined by 0.7% agarose gel with the TAE running buffer after 7-day irradiation (30 Gy) with Cs-131 or 18-day irradiation (30 Gy) with I-125. Plasmid DNA was damaged after both 7- and 18-day irradiation. *Lane:* 1 and 3, Plasmid DNA without irradiation; 2, plasmid DNA after 7-day irradiation (30 Gy) with Cs-131; 4, plasmid DNA after 18-day irradiation (30 Gy) with I-125. The *dotted rectangle* highlighted the damage of the plasmid DNA.

The high stability of RNA 3WJ nanoparticles in the presence of high concentration of denaturing agents (Fig. 3A) is a remarkable advantage for *in vivo* applications, including radiation therapy, because remaining intact *in vivo* and being resistant to various denaturing factors will be crucial for fulfilling the nanoparticle's designated function after injection into the body. Moreover, the determined melting temperature of the 3WJ RNA nanoparticles (Fig. 1D) is approximately two times higher than the normal human body temperature (37°C), which also indicates that this physical

Table 1. Results of I-125 Irradiation

Test	*Dose (Gy)*	S_k *(U)*	*Time (day)*	*RNA change*	*DNA change*
1	1	1.4	1	N	N
2	30	1.7	18	N	Y

N, no; Y, yes.

Table 2. Results of Cs-131 Irradiation

Test	*Dose (Gy)*	S_k *(U)*	*Time (day)*	*RNA change*	*DNA change*
1	7	0.98	7	N	N
2	20	1.47	20	N	Y
3	30	4.03	7	N	Y
4	90	8.57	11	N	Y

property of the RNA 3WJ nanoparticles is favorable for *in vivo* applications, including radiation therapy, because these RNA nanoparticles should not disassociate within the normal human body temperature range. Furthermore, the property of resistance to serum-induced degradation (Fig. 3B) suggests that these 2′F-modified RNA nanoparticles will also stay intact within the human body and, again, should be favorable as a targeted delivery system for *in vivo* cancer therapy.

The principle of radiation therapy is to use radiation to break DNA helical structures in the cancer cells. However, RNA has similar structures. To be able to carry radioisotopes, RNA structures should keep intact with the radiation. The study has shown that, unlike DNA, RNA nanoparticles were resistant to the radiation of I-125 or Cs-131 and remained stable under irradiation with therapeutic doses (Fig. 3C and D and Tables 1 and 2). This indicates that RNA nanoparticles are feasible to carry the radioisotope to kill cancer cells while remaining intact. The stability of the RNA nanoparticles under irradiation over a long time is important since the chemical conjugation of radioactive isotopes to RNA might be a time-consuming process depending on the rate and efficiency of the conjugation reaction. In the future experiments, we will also study the stability of RNA nanoparticles inside tumor tissues and try to develop the method to control the degradation of RNA nanoparticles as well as the release of radioisotope inside the tumor. In addition, I-125 and Cs-131 are gamma-emitters and the presence of gamma-emission is helpful in imaging and studying the biodistribution of the radiopharmaceutical for estimation of patient-specific dose distribution [60]. This is an advantage that gamma-emitters have over the pure beta-emitters like Y-90. In the absence of gamma-emission, surrogate isotopes like In-111 have to be used for internal dosimetry for pure alpha- or beta-emitters such as Y-90. Compared to I-131 that also emits photons, I-125 and Cs-131 have much lower energies and are easy for radiation protection. Although image quality for I-125 or Cs-131 will be affected by the low energies of photons, good quality I-125 images have been obtained using the gamma-camera [61,62]. Therefore, RNA nanoparticles carrying I-125 or Cs-131 have the potential to be used for accurate targeted radiation therapy.

It should be, however, noted that the sealed I-125 and Cs-131 sources used in this study were not carried by RNA nanoparticles. To be carried by RNA nanoparticles, unsealed I-125 or Cs-131 should be used to label RNA nanoparticles. The I-125- or Cs-131-labeled RNA nanoparticles will be injected into the patient body to target the tumor, and the radiation from I-125 or Cs-131 can thus kill the cancer cells guided by the nanoparticles. The I-125/Cs-131-labeled RNA particles will stay inside the tumor cells to deposit almost all the dose produced by I-125/Cs-131. Considering that the blood circulation time for humans is about 1 min compared to the half-life of I-125/Cs-131 of about 60 days/10 days, the dose lost during circulation is negligible. Detailed discussion of I-125/Cs-131-labeled RNA particles will be addressed in our future study. Based on the biodistribution study of pRNA nanoparticles published by Abdelmawla *et al.* [28], we expected that 3WJ nanoparticles labeled with radioisotope will also have a favorable biodistribution profile with similar tumor-targeting efficiency as the previously reported pRNA nanoparticles. In the future experiments, we will radioactively label 3WJ RNA nanoparticles and use the radioactive signal to quantify the doses delivered in individual organs and tumor. We will also compare the delivered dose to that provided by brachytherapy implanted sources.

Conclusions

Chemically modified RNA nanoparticles derived from pRNA 3WJ of phi29 DNA-packaging motor were resistant to the radiation of I-125 or Cs-131 and remained stable under irradiation with therapeutic doses over a significantly long time up to 20 days. Therefore, RNA 3WJ nanoparticles have the potential to carry I-125 or Cs-131 for targeted radiation therapy.

Acknowledgments

The research was partially supported by NIH grants EB019036, EB003730, and CA151648 to Peixuan Guo and the confocal microscopy shared resource of the University of Kentucky Markey Cancer Center, P30CA177558. The content is solely the responsibility of the authors and does not necessarily represent the official views of NIH. Funding to Peixuan Guo's Endowed Chair in the Nanobiotechnology position is by the William Fairish Endowment Fund. AFM images were prepared by Luda Shlyakhtenko and Yuri Lyubchenko using the Nanoimaging Core Facility at the University of Nebraska Medical Center. The authors thank Prakash Aryal and Ulrich Langner for help with I-125/Cs-131 preparation, and thank Emil F. Khisamutdinov for help with the TGGE experiment. Peixuan Guo is a cofounder of Kylin Therapeutics, Inc., and Biomotor and RNA Nanotechnology Development Corp. Ltd.

Author Disclosure Statement

Peixuan Guo is a cofounder of Kylin Therapeutics, Inc., and Biomotor and RNA Nanotechnology Development Corp. Ltd.

References

1. Hanahan D and RA Weinberg. (2000). The hallmarks of cancer. Cell 100:57–70.
2. Hanahan D and RA Weinberg. (2011). Hallmarks of cancer: the next generation. Cell 144:646–674.
3. Jemal A, F Bray, MM Center, J Ferlay, E Ward and D Forman. (2011). Global cancer statistics. CA Cancer J Clin 61:69–90.
4. Economic Impact of Cancer. www.cancer.org/cancer/cancerbasics/economic-impact-of-cancer. Last accessed date: April 20, 2015.
5. Baskar R, KA Lee, R Yeo and KW Yeoh. (2012). Cancer and radiation therapy: current advances and future directions. Int J Med Sci 9:193–199.
6. Bloomer WD and S Hellman. (1975). Normal tissue responses to radiation therapy. N Engl J Med 293:80–83.
7. Bentzen SM. (2006). Preventing or reducing late side effects of radiation therapy: radiobiology meets molecular pathology. Nat Rev Cancer 6:702–713.
8. Spencer RP, RH Seevers, and AM Friedman, eds. (1987). *Radionuclides in Therapy*. CRC Press, Boca Raton, FL.
9. Peer D, JM Karp, S Hong, OC Farokhzad, R Margalit and R Langer. (2007). Nanocarriers as an emerging platform for cancer therapy. Nat Nanotechnol 2:751–760.

10. Davis ME, ZG Chen and DM Shin. (2008). Nanoparticle therapeutics: an emerging treatment modality for cancer. Nat Rev Drug Discov 7:771–782.
11. Brannon-Peppas L and JO Blanchette. (2004). Nanoparticle and targeted systems for cancer therapy. Adv Drug Deliv Rev 56:1649–1659.
12. Lee H, AK Lytton-Jean, Y Chen, KT Love, AI Park, ED Karagiannis, A Sehgal, W Querbes, CS Zurenko, *et al.* (2012). Molecularly self-assembled nucleic acid nanoparticles for targeted in vivo siRNA delivery. Nat Nanotechnol 7:389–393.
13. Guo P. (2010). The emerging field of RNA nanotechnology. Nat Nanotechnol 5:833–842.
14. Shu Y, F Pi, A Sharma, M Rajabi, F Haque, D Shu, M Leggas, BM Evers and P Guo. (2014). Stable RNA nanoparticles as potential new generation drugs for cancer therapy. Adv Drug Deliv Rev 66C:74–89.
15. Kairemo K, P Erba, K Bergstrom and E Pauwels. (2008). Nanoparticles in cancer. Curr Radiopharm 1:30–36.
16. Cai W, T Gao, H Hong and J Sun. (2008). Applications of gold nanoparticles in cancer nanotechnology. Nanotechnol Sci Appl 1:17–32.
17. Zhang L, H Chen, L Wang, T Liu, J Yeh, G Lu, L Yang and H Mao. (2010). Delivery of therapeutic radioisotopes using nanoparticle platforms: potential benefit in systemic radiation therapy. Nanotechnol Sci Appl 3:159–170.
18. Shu Y, M Cinier, D Shu and P Guo. (2011). Assembly of multifunctional phi29 pRNA nanoparticles for specific delivery of siRNA and other therapeutics to targeted cells. Methods 54:204–214.
19. Haque F, D Shu, Y Shu, L Shlyakhtenko, P Rychahou, M Evers and P Guo. (2012). Ultrastable synergistic tetravalent RNA nanoparticles for targeting to cancers. Nano Today 7:245–257.
20. Shu Y, F Haque, D Shu, W Li, Z Zhu, M Kotb, Y Lyubchenko and P Guo. (2013). Fabrication of 14 different RNA nanoparticles for specific tumor targeting without accumulation in normal organs. RNA 19:766–777.
21. Guo P, C Zhang, C Chen, M Trottier and K Garver. (1998). Inter-RNA interaction of phage phi29 pRNA to form a hexameric complex for viral DNA transportation. Mol Cell 2:149–155.
22. Guo P, F Haque, B Hallahan, R Reif and H Li. (2012). Uniqueness, advantages, challenges, solutions, and perspectives in therapeutics applying RNA nanotechnology. Nucleic Acid Ther 22:226–245.
23. Bindewald E, K Afonin, L Jaeger and BA Shapiro. (2011). Multistrand RNA secondary structure prediction and nanostructure design including pseudoknots. ACS Nano 5:9542–9551.
24. Ye X, M Hemida, HM Zhang, P Hanson, Q Ye and D Yang. (2012). Current advances in Phi29 pRNA biology and its application in drug delivery. Wiley Interdiscip Rev RNA 3:469–481.
25. Afonin KA, EO Danilov, IV Novikova and NB Leontis. (2008). TokenRNA: A new type of sequence-specific, label-free fluorescent biosensor for folded RNA molecules. Chembiochem 9:1902–1905.
26. Shu D, WD Moll, Z Deng, C Mao and P Guo. (2004). Bottom-up assembly of RNA arrays and superstructures as potential parts in nanotechnology. Nano Lett 4:1717–1723.
27. Shu D, Y Shu, F Haque, S Abdelmawla and P Guo. (2011). Thermodynamically stable RNA three-way junctions for constructing multifuntional nanoparticles for delivery of therapeutics. Nat Nanotechnol 6:658–667.
28. Abdelmawla S, S Guo, L Zhang, S Pulukuri, P Patankar, P Conley, J Trebley, P Guo and QX Li. (2011). Pharmacological characterization of chemically synthesized monomeric pRNA nanoparticles for systemic delivery. Mol Ther 19:1312–1322.
29. Cerchia L, PH Giangrande, JO McNamara and FV de. (2009). Cell-specific aptamers for targeted therapies. Methods Mol Biol 535:59–78.
30. Guo P and M Trottier. (1994). Biological and biochemical properties of the small viral RNA (pRNA) essential for the packaging of the double-stranded DNA of phage φ29. Semin Virol 5:27–37.
31. Rajendran JG. (2007). Therapeutic radioisotopes. In: *Nuclear Medicine Therapy*. Early J and W Brenner, eds. Informa Healthcare, New York, NY, pp 9–20.
32. Hoefnagel CA. (1998). Radionuclide cancer therapy. Ann Nucl Med 12:61–70.
33. Sofou S. (2008). Radionuclide carriers for targeting of cancer. Int J Nanomedicine 3:181–199.
34. Hamoudeh M, MA Kamleh, R Diab and H Fessi. (2008). Radionuclides delivery systems for nuclear imaging and radiotherapy of cancer. Adv Drug Deliv Rev 60:1329–1346.
35. Williams LE, GL DeNardo and RF Meredith. (2008). Targeted radionuclide therapy. Med Phys 35:3062–3068.
36. Lyubchenko YL and LS Shlyakhtenko. (2009). AFM for analysis of structure and dynamics of DNA and protein-DNA complexes. Methods 47:206–213.
37. Pieken WA, DB Olsen, F Benseler, H Aurup and F Eckstein. (1991). Kinetic characterization of ribonuclease-resistant 2′-modified hammerhead ribozymes. Science 253: 314–317.
38. Kawasaki AM, MD Casper, SM Freier, EA Lesnik, MC Zounes, LL Cummins, C Gonzalez and PD Cook. (1993). Uniformly modified 2′-deoxy-2′-fluoro phosphorothioate oligonucleotides as nuclease-resistant antisense compounds with high affinity and specificity for RNA targets. J Med Chem 36:831–841.
39. Sabahi A, J Guidry, GB Inamati, M Manoharan and P Wittung-Stafshede. (2001). Hybridization of 2′-ribose modified mixed-sequence oligonucleotides: thermodynamic and kinetic studies. Nucleic Acids Res 29:2163–2170.
40. Liu J, S Guo, M Cinier, LS Shlyakhtenko, Y Shu, C Chen, G Shen and P Guo. (2011). Fabrication of stable and RNase-resistant RNA nanoparticles active in gearing the nanomotors for viral DNA packaging. ACS Nano 5: 237–246.
41. Meigooni AS, JL Hayes, H Zhang and K Sowards. (2002). Experimental and theoretical determination of dosimetric characteristics of IsoAid ADVANTAGE 125I brachytherapy source. Med Phys 29:2152–2158.
42. Prestidge BR, WS Bice, I Jurkovic, E Walker, S Marianne and A Sadeghi. (2005). Cesium-131 permanent prostate brachytherapy: an initial report. Int J Radiat Oncol Biol Phys 63:S336–S337.
43. Ravi A, BM Keller and J Pignol. (2011). Evaluation of the radiation safety of using Cs-131 seeds for permanent breast seed implantation. Int J Radiat Oncol Biol Phys 81:S720–S721.
44. Yan W, S Trichter, A Sabbas, AG Wernicke, D Nori, KSC Chao and B Parashar. (2010). Cesium-131 brachytherapy for lung cancer: dosimetric, safety considerations

and initial experience. Int J Radiat Oncol Biol Phys 78: S540–S541.
45. Rivard MJ, CS Melhus, S Sioshansi and J Morr. (2008). The impact of prescription depth, dose rate, plaque size, and source loading on the central axis using Pd-103, I-125, and Cs-131. Brachytherapy 7:327–335.
46. Luo W, J Molloy, P Aryal, J Feddock and M Randall. (2014). Determination of prescription dose for Cs-131 permanent implants using the BED formalism including resensitization correction. Med Phys 41:024101.
47. Wooten CE, M Randall, J Edwards, P Aryal, W Luo and J Feddock. (2014). Implementation and early clinical results utilizing Cs-131 permanent interstitial implants for gynecologic malignancies. Gynecol Oncol 133:268–273.
48. Murphy MK, RK Piper, LR Greenwood, MG Mitch, PJ Lamperti, SM Seltzer, MJ Bales and MH Phillips. (2004). Evaluation of the new cesium-131 seed for use in low-energy x-ray brachytherapy. Med Phys 31:1529–1538.
49. Rosenbaum V and D Riesner. (1987). Temperature-gradient gel-electrophoresis - thermodynamic analysis of nucleic-acids and proteins in purified form and in cellular-extracts. Biophys Chem 26:235–246.
50. Binzel DW, EF Khisamutdinov and P Guo. (2014). Entropy-driven one-step formation of Phi29 pRNA 3WJ from three RNA fragments. Biochemistry 53:2221–2231.
51. Guo P. (2005). RNA nanotechnology: engineering, assembly and applications in detection, gene delivery and therapy. J Nanosci Nanotechnol 5:1964–1982.
52. Guo P and F Haque, eds. (2013). *RNA Nanotechnology and Therapeutics*. CRC Press, Boca Raton, FL.
53. Khisamutdinov EF, DL Jasinski and P Guo. (2014). RNA as a boiling-resistant anionic polymer material to build robust structures with defined shape and stoichiometry. ACS Nano 8:4771–4781.
54. Jasinski D, EF Khisamutdinov, YL Lyubchenko and P Guo. (2014). Physicochemically tunable poly-functionalized rna square architecture with fluorogenic and ribozymatic properties. ACS Nano 8:7620–7629.
55. Khisamutdinov E, H Li, D Jasinski, J Chen, J Fu and P Guo. (2014). Enhancing immunomodulation on innate immunity by shape transition among RNA triangle, square, and pentagon nanovehicles. Nucleic Acids Res 42:9996–10004.
56. Lee TJ, F Haque, D Shu, JY Yoo, H Li, RA Yokel, C Horbinski, TH Kim, S-H Kim, *et al.* (2015). RNA nanoparticles as a vector for targeted siRNA delivery into glioblastoma mouse model. Oncotarget [Epub ahead of print].
57. Afonin KA, M Viard, I Kagiampakis, CL Case, MA Dobrovolskaia, J Hofmann, A Vrzak, M Kireeva, WK Kasprzak and VN KewalRamani. (2014). Triggering of RNA interference with RNA – RNA, RNA – DNA, and DNA – RNA nanoparticles. ACS Nano 9:251–259.
58. Afonin KA, M Viard, AY Koyfman, AN Martins, WK Kasprzak, M Panigaj, R Desai, A Santhanam, WW Grabow, *et al.* (2014). Multifunctional RNA nanoparticles. Nano Lett 14:5662–5671.
59. Jensen SA, ES Day, CH Ko, LA Hurley, JP Luciano, FM Kouri, TJ Merkel, AJ Luthi, PC Patel, *et al.* (2013). Spherical nucleic acid nanoparticle conjugates as an RNAi-based therapy for glioblastoma. Sci Transl Med 5:209ra152.
60. Lee FT, A Rigopoulos, C Hall, K Clarke, SH Cody, FE Smyth, Z Liu, MW Brechbiel, N Hanai, *et al.* (2001). Specific localization, gamma camera imaging, and intracellular trafficking of radiolabelled chimeric anti-G(D3) ganglioside monoclonal antibody KM871 in SK-MEL-28 melanoma xenografts. Cancer Res 61:4474–4482.
61. Zinn KR, TR Chaudhuri, VN Krasnykh, DJ Buchsbaum, N Belousova, WE Grizzle, DT Curiel and BE Rogers. (2002). Gamma camera dual imaging with a somatostatin receptor and thymidine kinase after gene transfer with a bicistronic adenovirus in mice. Radiology 223:417–425.
62. Meng LJ, G Fu, EJ Roy, B Suppe and CT Chen. (2009). An ultrahigh resolution SPECT system for I-125 mouse brain imaging studies. Nucl Instrum Methods Phys Res A 600:498–505.

Address correspondence to:
Wei Luo, PhD
Department of Radiation Medicine
Markey Cancer Center
University of Kentucky
Lexington, KY 40536

E-mail: wei.luo@uky.edu

Peixuan Guo, PhD
Department of Pharmaceutical Sciences
College of Pharmacy
University of Kentucky
Lexington, KY 40536

E-mail: peixuan.guo@uky.edu

Received for publication December 5, 2014; accepted after revision April 20, 2015.